LAURI KALDAMÄE

Fermion mass and spin polarisation effects in top quark pair production and the decay of the Higgs boson

TARTU ÜLIKOOL · UNIVERSITAS TARTUENSIS

1632

DISSERTATIONES PHYSICAE UNIVERSITATIS TARTUENSIS

109

LAURI KALDAMÄE

Fermion mass and spin polarisation effects in top quark pair production and the decay of the Higgs boson

This study was carried out at the University of Tartu.

The dissertation was admitted on 04.04.2017 in partial fulfilment of the requirements for the degree of Doctor of Philosophy in Physics, and was allowed for defence by the Council of the Institute of Physics, University of Tartu.

Supervisor: Dr. habil. Stefan Groote
    senior scientist at the Institute of Physics, University of Tartu, Estonia

Opponents: Dr. habil. Markus Diehl
    Staff scientist at DESY, Hamburg, Germany
  PhD Kristjan Kannike
    senior scientist at the National Institute of Chemical Physics and Biophysics, Tallinn, Estonia

Defence: 17.05.2017

Table of Contents

List of publications

This thesis is based on the following publications which are referred to in the text by their Roman numerals. The full texts are included at the end of the thesis.

I L. Kaldamäe, S. Groote, J. G. Körner, Analytical $O(\alpha_s)$ corrections to the beam frame double-spin density matrix elements of $e^+e^- \to t\bar{t}$, Physical Review **D94** (2016) 114003

II L. Kaldamäe, S. Groote, Virtual and real processes, the Källén function, and the relation to dilogarithms, Journal of Physics G: Nuclear and Particle Physics **42** (2015) 085003

III S. Berge, S. Groote, J. G. Körner, L. Kaldamäe, Lepton-mass effects in the decays $H \to ZZ^* \to \ell^+\ell^-\tau^+\tau^-$ and $H \to WW^* \to \ell\nu\tau\nu_\tau$, Physical Review **D92** (2015) 033001

Author's contribution

The author was the main contributor to article I and was responsible for the calculation, the diagrams, the analysis and the manuscript. Article II was a joint project where the author contributed to the calculation, to the diagrams and to the manuscript. In article III the author contributed to the numerical calculations and to the diagrams.

A remark about the structure of this thesis

This thesis is built upon articles I, II, and III. These articles are integral parts of the thesis. Therefore, if one should aim to achieve an exhaustive understanding of the topic, the main text should be read together with the attached publications.

1 Introduction

The modern description of everything regarding elementary particles and their interactions is given by the Standard Model of particle physics. The Standard Model is based on quantum field theories.

Quantum field theory combines three of the major themes of modern physics: quantum theory, the field concept, and the principle of relativity. Quantum field theory describes modern elementary particle physics and supplies essential tools to nuclear physics, atomic physics, condensed matter physics, and astrophysics [1].

The Standard Model excels in experimental precision, having some results known up to 13 significant figures (for instance, QED prediction for the magnetic moment of the electron [2]).

On the way from classical quantities like position, momentum, time, and energy to the quantum observables which are described by wave functions and operators, quantum field theory is essential for a modern understanding of the concept of particle–field duality. Initially the wave functions were classical fields which described the probability distributions of kinematics of individual particles. However, the substantial addition of quantum theory led to the quantification of these fields which enabled them to describe systems of multiple particles. This is known as the canonical quantisation, which is in essence the principle that multi-particle states are created from the vacuum state via creation and annihilation operators.

Starting from a few specific relativistic field equations (Klein–Gordon, Dirac, Maxwell, and Proca equations), scalar bosons (e.g. Higgs boson), fermions (e.g. electron and quarks), and vector bosons (e.g. photon, W and Z bosons) could be described. In quantum field theory these various particle types contribute to the Lagrangian, from which differential equations evolve via the Euler–Lagrange formalism, describing the propagation of the fields. On this way through quantisation of particles and fields we arrived at the pinnacle of our understanding of elementary particles and their interactions – the quantum field theory.

The vector bosons were introduced via gauge theory. For the field operators to be invariant under a phase transformation, a gauge field needs to be added which is connected to the initial field operator via the interaction contribution. All known vector bosons are gauge bosons, although their connection to fermions may not be as simple as the photon's connection to fermions which is given by the electric charges of the fermions. Gauge theories are based on group theory, and semisimple Lie groups and algebras are appropriate tools to describe interactions. This led to the development of theories for the strong interaction (quantum chromodynamics, $SU(3)$), the electroweak interaction

(Glashow–Weinberg–Salam theory, $SU(2) \times U(1)$), and the Higgs mechanism which describes how particles feel their inertial mass through spontaneous symmetry breaking.

It would be beneficial to solve the quantum system described by the Lagrangian as a whole, as it is possible in some specific classical cases, but unfortunately this is not possible in case of quantum field theory. However, if one considers the strength of interaction in a certain kinematic region one can expand the interaction into a series. For example, in the short range (due to asymptotic freedom) the strong interaction is relatively weak, but in case of the larger range (due to confinement) the interaction is much stronger. If one expands the interaction into a series, one obtains contributions of different orders, the strength of which is decreasing gradually. This enables one to calculate a process with relative ease and to add minute so-called radiative corrections with increasing complexity and decreasing significance. If the interaction is weak enough, the leading order (LO) and the next-to-leading order (NLO) contributions often give a clue about how well the series converges. This is the reason why in this work only radiative corrections up to NLO are considered.

Richard P. Feynman developed an excellent tool for the calculation of the series which is also named after him. A Feynman diagram contains a large part of the important information about the process of interest in a simple and easy-to-understand visual way. Every interaction is visualised as a connection point of lines (vertex), and the movement of a free particle is visualised as a line connecting the vertices (propagator). External lines describe initial and final states of particles. The Feynman rules give us a procedure for assembling these elements into a process and interpreting the diagram mathematically. Such a diagram also gives us a way to visually evaluate the types of interactions involved in the process.

The elements of the Feynman diagrams are mathematically translated into contributions to the matrix element which in turn is related to experimentally measurable quantities. If the process of interest is a decay process (as in article III), the decay width is measured. If the process is a scattering event (as in article I), the scattering cross section is measured. These quantities that depend (either explicitly or indirectly) on kinematic variables enable us to find expectation values which determine the values of macroscopic quantities like momentum or polarisation.

2 Preface to $t\bar{t}$ spin correlation

2.1 Overview

Article I presents analytical results for $O(\alpha_s)$ corrections to the double spin density matrix elements in the reaction $e^+e^- \to t\bar{t}$. These results are related to the research planned for the scheduled linear collider projects (ILC and CLIC). Studying the top quark and the Higgs boson are two of the main reasons why new e^+e^- colliders are considered [3, 4].

Hadron colliders and e^+e^- colliders have intrinsically different settings for studying heavy quarks. For other heavy quarks like c and b quarks, there have been experiments in both types of colliders, but top quarks have been studied up to now only in hadron colliders, because the pair production threshold of the top quark is around 350 GeV, higher than the center of mass energy of any e^+e^- collider that has operated so far [3]. This explains the need to study top quark production at a e^+e^- collider. Compared to the LHC, there are advantages for studying top quark in e^+e^- colliders such as cleanliness (low backgrounds), a high production rate for heavy particles, the simplicity of the experimental event topology, and a high accuracy of the theoretical calculations for the underlying processes [5].

One of the points of interest in e^+e^- colliders is the study of top quark production and decay. These measurements will make use of the accurate reconstruction of $t\bar{t}$ events to probe the full structure of the top quark coupling to electroweak interactions and provide excellent sensitivity to physics beyond the Standard Model [3]. Additionally, due to its mass, the top quark couples strongest to the Higgs field and, therefore, plays a central role in many Beyond-Standard Model models. Precision measurements of top-quark properties at e^+e^- colliders promise therefore to be highly sensitive to physics beyond the Standard Model [4].

2.2 Methodology

2.2.1 Cross section and Feynman rules to calculate it

We can start for example with the diagrams for the process $e^+e^- \to t\bar{t}$ which is examined in article I. The zeroth order (also known as the Born level) diagram is shown in Figure 1a.

We want to calculate the scattering cross section for this process. The differential cross section element $d\sigma$ is connected to the scattering matrix element $\mathcal{M}$ via

$$d\sigma = |\mathcal{M}|^2 dPS, \tag{1}$$

where the phase space element dPS stands for a generic phase space element
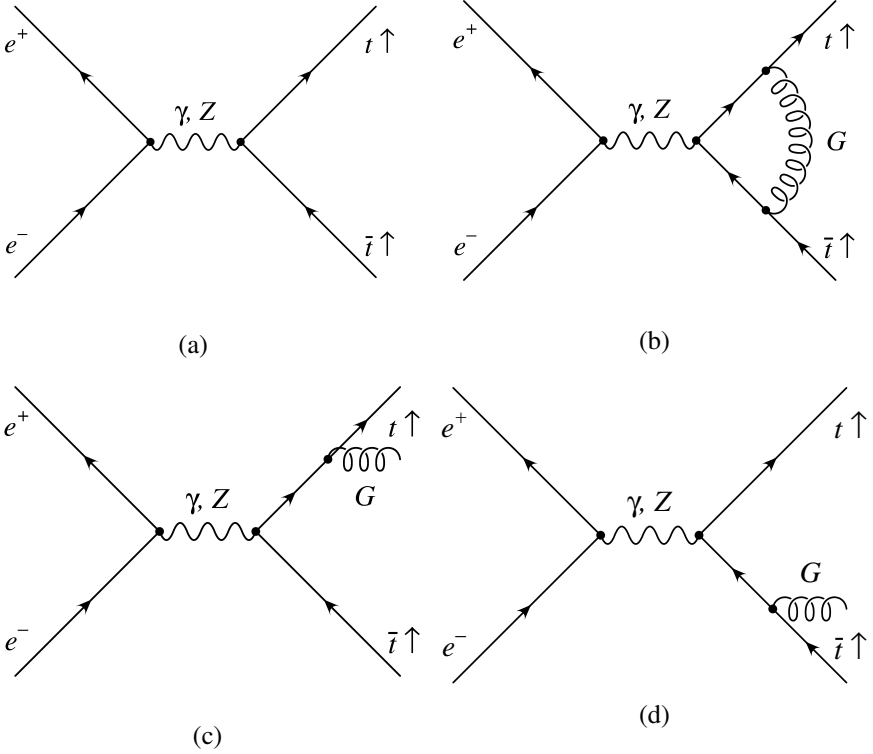
Figure 1: (a) The LO (Born term level) Feynman diagram, (b) NLO vertex correction, (c) and (d) NLO tree corrections to the Feynman diagram for the process $e^+e^- \to t\bar{t}$.

that remains after single or multiple phase space integrations. The square of the modulus $|\mathcal{M}|^2$ is the probability of this process happening when e^+ and e^- collide.

For this calculation we can use the following Feynman rules

$$-ie\gamma^\mu Q_f \qquad \text{fermion and photon vertex}$$

$$\frac{ie(v_f + a_f\gamma_5)\gamma^\mu}{2\sin(2\theta_W)} \qquad \text{fermion and } Z \text{ boson vertex}$$

$$-\frac{ig_{\mu\nu}}{q^2} \qquad \text{photon propagator}$$

$$-\frac{ig_{\mu\nu}}{q^2}\chi_Z(q^2) \qquad \text{Z boson propagator,} \qquad (2)$$

where e is the elementary charge, γ^μ are the Dirac gamma matrices, Q_f is the electric charge of the fermion to which the electroweak currents directly couple,

and v_f and a_f are the electroweak vector and axial vector coupling constants. For the top quark the vector and axial-vector couplings (in the Glashow–Weinberg–Salam model) are given by

$$v_t = 1 - \frac{8}{3} \sin^2 \theta_W \tag{3}$$

$$a_t = 1. \tag{4}$$

θ_W is the Weinberg (weak mixing) angle. χ_Z is the Breit–Wigner multiplier

$$\chi_Z(q^2) = \frac{g m_Z^2 q^2}{q^2 - m_Z^2 + i m_Z \Gamma_Z}, \tag{5}$$

where Γ_Z is the width (decay rate) of the Z boson, g is the interaction strength factor, and q is the boson momentum. Initial fermion and antifermion states are described by the spinors u and v, and final fermion and antifermion states are described by the adjoint spinors $\bar{u} = u^\dagger \gamma^0$ and $\bar{v} = v^\dagger \gamma^0$ respectively, which satisfy the completeness relations

$$u(p, s) \bar{u}(p, s) = \frac{1}{2}(1 + \gamma_5 \slashed{s})(\slashed{p} + m)$$

$$v(p, s) \bar{v}(p, s) = \frac{1}{2}(1 + \gamma_5 \slashed{s})(\slashed{p} - m), \tag{6}$$

where p is the momentum, m is the mass and s is the spin of the fermion. The slash notation $\slashed{p}$ and $\slashed{s}$ denote a sum of 4-vector components multiplied with respective gamma matrices,

$$\slashed{p} = \sum_{\mu=0}^{3} p_\mu \gamma^\mu = p_\mu \gamma^\mu. \tag{7}$$

For a more complete listing of Feynman rules see e.g. [6] (chapter 2.4.2.2 for QCD and Appendix A.2 for electroweak) and [7] (chapter 4).

The boson momentum is carried by the two neutral vector bosons of the electroweak theory, the photon and the Z boson. While the photon couples to the fermions via the vector coupling, for the Z boson the coupling is a mixture of vector and axial vector components. Before we dwell into this point, for simplicity we start with the photon only. We divide the calculation of the scattering matrix up into two parts, the lepton part (related to the electron and the positron on the left-hand side of the diagram) and the hadron part (related to the quarks on the right hand side of the diagram),

$$|\mathcal{M}|^2 = L_{\mu\nu} H^{\mu\nu}. \tag{8}$$

Taking the hadron part of the diagram of the LO (Born term level) process and taking into account how all the indices combine into a trace operator, we get a rather long expressions like for instance

$$H^{\mu\nu} = \text{Tr}(\frac{1}{2}(1 + \gamma^5 \slashed{s}_1)(\slashed{p}_1 + m)\gamma^\mu \frac{1}{2}(1 + \gamma^5 \slashed{s}_2)(\slashed{p}_2 - m)\gamma^\nu). \qquad (9)$$

The calculation of this kind of traces is extensive but highly systematical, thus we let a computer do all the work for us.

At this point one needs to specify kinematics, that is to give a specific frame of reference in which all vectors are described in terms of energies and angles. For example, θ is the angle between the directions of electron and top quark.

Generally there will be too many variables after the trace calculation. In order to get a reasonably interpretable result one has to integrate out the non-observed quantities. Only the "interesting" variables are left which in this case are the center-of-mass energy $\sqrt{q^2}$ and the cosine of the angle θ.

Finally we can add up the Born term level result with the NLO corrections (with appropriate general factors) to obtain an improved result for the angular dependence of the probability of this process at any examined energy. (See Figures 1 through 7 in article I.)

2.2.2 Vector and axial vector contributions

The calculation employed for evaluating $t\bar{t}$ spin–spin correlation follows the same pattern as the example in section 2.2.1. To distinguish between vector and axial vector contributions (the latter appear only in case of the Z boson) in a trace expression like in equation (9) we add upper indices V and A which denote the substitution of γ^μ (V) with $\gamma^5 \gamma^\mu$ (A). This shortens the Z boson contribution, as part of it repeats the photon contribution. The hadron tensor components H^{AA}, H^{AV}, H^{VA} and H^{VV} corresponding to vector and axial vector vertices are redistributed into different tensor components

$$H_\alpha^1 = \frac{1}{2}(H_\alpha^{VV} + H_\alpha^{AA}), \qquad H_\alpha^2 = \frac{1}{2}(H_\alpha^{VV} - H_\alpha^{AA}),$$

$$H_\alpha^3 = \frac{i}{2}(H_\alpha^{VA} - H_\alpha^{AV}), \qquad H_\alpha^4 = \frac{1}{2}(H_\alpha^{VA} + H_\alpha^{AV}). \qquad (10)$$

The same is done for the corresponding components L^{VV}, L^{VA}, L^{AV} and L^{AA}. This allows us to reassemble the entire cross–section via the electroweak coupling matrix $g_{ij}(q^2)$ (for explicit terms see [8]):

$$|\mathcal{M}|^2 = \Sigma \, L_{\mu\nu}^i g_{ij} H^{j\,\mu\nu}. \qquad (11)$$

This scheme has also been used in earlier works (for example [9]) and describes the result by large parts H^1, H^4 and small parts H^2, H^3.

2.2.3 NLO correction and regularisation

In the calculation of $e^+e^- \to t\bar{t}$, the NLO corrections shown in Figures 1b, 1c, and 1d were also taken into account. Even though the Born term level diagram (Figure 1a) and the first order loop diagram (Figure 1b) contribute to a different (two-particle) phase space than the first order tree diagrams (three-particle phase space, Figures 1c and 1d), they are inextricably related to each other and will be dealt with together in this work. The reason is that the Lee–Nauenberg theorem predicts the cancellation of infrared (IR) singularities between the two first order parts. It is worth to note that the majority of work done on the calculations of article I has gone into evaluating integrals arising from tree correction (Figure 1c and 1d). These integrals tend to be infinite and thus need to be carefully handled to cancel all the infinities, because the final result must be finite.

The basic integrals have the structure

$$I_{n_y n_z}(m_y, m_z) = \int_{y_-}^{y_+} dy \int_{z_-(y)}^{z_+(y)} dz\, y^{m_y} z^{m_z} R_y^{n_y} R_z^{n_z}, \tag{12}$$

where $R_y = \sqrt{(1-y)^2 - \xi}$, $R_z = \sqrt{(1-z)^2 - \xi}$ and $\xi = 4m^2/q^2$. The integrals with $m_y + m_z = -2$ are IR singular. For the regularisation of the IR singularity at $y = z = 0$ we use a finite gluon mass $m_G = \sqrt{\Lambda q^2}$ with infinitesimally small parameter Λ. The subtraction of the singularity is performed by adding and subtracting an integral with the same singular behaviour but with a simpler integrand. The simplified integrand is obtained from the original integrand by an expansion around $y = 0$. In this expansion, both R_y and R_z are replaced by $\sqrt{1-\xi}$, leading to generic divergent parts.

2.2.4 Observables and reference frames

The cross section is connected to observables. The observables in question include the polarisation of the particles. The spin polarisation is an inherent quantum effect derived from the spin. Therefore, a consideration of spin states is in order here [10].

If we have a mixture of pure states

$$|\psi^{(i)}\rangle = \sum_{m=-s}^{s} c_m |sm\rangle \tag{13}$$

each with probability $p^{(i)}$ ($\sum_i p^{(i)} = 1$) and an arbitrary operator $\mathcal{O}$ with matrix elements

$$\mathcal{O}_{mm'} = \langle m|\mathcal{O}|m'\rangle, \tag{14}$$

the mean value over the entire ensemble of states $|\psi^{(i)}\rangle$ given by

$$\langle \mathcal{O} \rangle = \sum_i p^{(i)} \langle \mathcal{O} \rangle_{\psi^{(i)}} = \sum_i p^{(i)} \sum_{m,m'} c_{m'}^{(i)*} \mathcal{O}_{m'm} c_m^{(i)}$$

$$= \sum_{m,m'} \mathcal{O}_{m'm} \sum_i p^{(i)} c_{m'}^{(i)*} c_m^{(i)} = \sum_{m,m'} \mathcal{O}_{m'm} \rho_{mm'} = \mathrm{Tr}(\hat{\rho}\mathcal{O}). \qquad (15)$$

Therefore, the mean value $\langle \mathcal{O} \rangle$ of the arbitrary operator $\mathcal{O}$ is obtained by calculating the trace $Tr(\hat{\rho}\mathcal{O})$ with the spin density matrix $\hat{\rho}$ with components

$$\rho_{mm'} = \sum_i p^{(i)} c_{m'}^{(i)*} c_m^{(i)}. \qquad (16)$$

In case of two polarised top quarks in the final state, the polarisation observables are described in terms of the spin density matrix, and the spin–spin correlation in terms of the double spin density matrix. The 4×4 unnormalised double density matrix $\hat{\rho}$ is parametrised by expanding it in outer products of the standard set of 2×2 matrices:

$$\hat{\rho} = (\hat{\rho}_{\lambda_1\lambda_2,\lambda_1'\lambda_2'}) = \frac{1}{4}\left(\rho\,\mathbb{1} \otimes \mathbb{1} + \rho^{e_1^i}\sigma_i \otimes \mathbb{1} + \rho^{\bar{e}_2^j}\mathbb{1} \otimes \sigma_j + \rho^{e_1^i\bar{e}_2^j}\sigma_i \otimes \sigma_j\right), \qquad (17)$$

where $\vec{e}_1$ and $\vec{e}_2$ describe spin quantisation axes, σ are Paul matrices, and the outer product symbol $\otimes$ denotes the tensor product between the spin states of top and antitop quark according to $(A \otimes B)_{\lambda_1\lambda_2,\lambda_1'\lambda_2'} = A_{\lambda_1\lambda_1'}B_{\lambda_2\lambda_2'}$. The labels λ_1 (λ_1') and λ_2 (λ_2') denote the two spin states of the top and antitop quark, respectively.

There are several possible ways to define spin quantisation axes. As in Refs. [11, 12] we choose to attach the reference frame to the top quark rest frame (or the beam frame). Forming an orthonormal triplet as in Ref. [13], the basis vectors are defined via the directions of the momenta of top quark and electron (see Figure 2),

$$\hat{t} = \frac{(\vec{p}_{e-} \times \vec{p}_t) \times \vec{p}_t}{|(\vec{p}_{e-} \times \vec{p}_t) \times \vec{p}_t|}, \qquad \hat{n} = \frac{\vec{p}_{e-} \times \vec{p}_t}{|\vec{p}_{e-} \times \vec{p}_t|}, \qquad \hat{l} = \frac{\vec{p}_t}{|\vec{p}_t|}. \qquad (18)$$

Another possible orthonormal frame is the event frame, in which the basis vectors do not depend on the direction of the electron momentum but instead are defined via the directions of top and antitop quark momenta,

$$\hat{T} = \frac{(\vec{p}_t \times \vec{p}_{\bar{t}}) \times \vec{p}_t}{|(\vec{p}_t \times \vec{p}_{\bar{t}}) \times \vec{p}_t|}, \qquad \hat{N} = \frac{\vec{p}_t \times \vec{p}_{\bar{t}}}{|\vec{p}_t \times \vec{p}_{\bar{t}}|}, \qquad \hat{L} = \frac{\vec{p}_t}{|\vec{p}_t|} \qquad (19)$$

The analytical results of calculations are somewhat more complicated in this case, as they contain additionally elliptic functions. The results have still to be published.
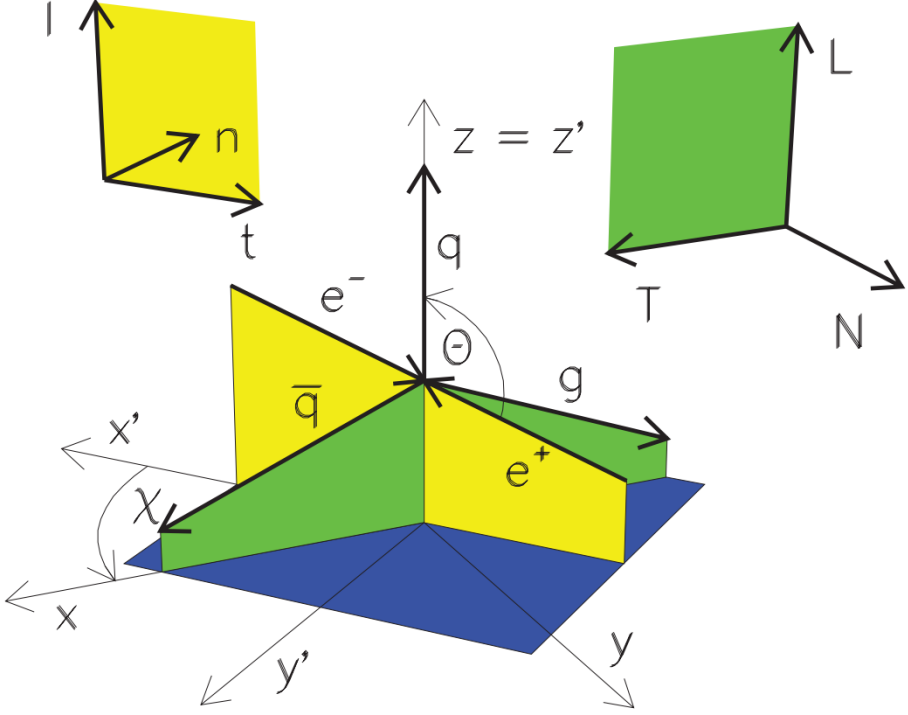
Figure 2: The orthonormal bases.

2.3 Results

The aim of calculating the spin–spin correlations of the top–antitop quark pair was to find analytical expressions which describe these correlations. The originality of these results stems from the inclusion of mass and spin polarisation effects. Analytical results enable us to study the dependence of the result on masses, initial beam polarisations and other parameters and to determine the limiting behaviour in different kinematical cases.

The coefficients $\rho^{e_1^i \bar{e}_2^j}$ in equation (17) describe the spin–spin correlation and are given as an analytical result in Appendix B of article I. However, these are not the actual quantities observed in experiments. The quark polarisation can be deduced from analysing the angular distribution of subsequent quark decay directly in the quark rest frame [14, 15].

The coefficients $\rho^{e_1^i \bar{e}_2^j}$ are incorporated into observables. Following the ideas from Refs. [11, 12], the observables are defined as

$$O^{e_1 e_2} = \frac{d\sigma^{e_1 e_2}}{d\sigma}, \tag{20}$$

where $\vec{e}_1$ and $\vec{e}_2$ are elements of the *same* frame, i.e. the top quark rest frame, and are selected from the basis in (18). The cross section rate for observables in (20) is calculated via the double spin density matrix $\hat{\rho}$ according to

$$d\sigma^{e_1 e_2} \;=\; \frac{1}{2q^2}\,\mathrm{Tr}\left(\hat{\rho}\, e_1^i\frac{1}{2}\sigma_i \otimes e_2^j\frac{1}{2}\sigma_j\right)dPS \;=\; \frac{1}{2q^2}\rho^{e_1 e_2}dPS, \quad (21)$$

and the unpolarised normalisation rate can be calculated by

$$d\sigma \;=\; \frac{1}{2q^2}\,\mathrm{Tr}\left(\hat{\rho}\,\mathbb{1}\otimes\mathbb{1}\right)dPS \;=\; \frac{1}{2q^2}\rho\,dPS. \quad (22)$$

The analytic results for the NLO $O(\alpha_s)$ contributions to the correlation matrix are given in terms of the three unit vectors $\hat{t}$, $\hat{n}$ and $\hat{l}$ in the laboratory frame. The detailed results have to be combined with the electroweak form factors (see Eq. (11)) to obtain

$$\rho^{P_1 P_2} = \sum_{i,j=1}^{4} g_{ij}\rho_{ij}^{P_1 P_2} \qquad P_1, P_2 \in \{t, n, l\}. \quad (23)$$

$\rho_{ij}^{P_1 P_2}$ is divided up into five different angular dependencies,

$$
\begin{aligned}
\rho_{ij}^{P_1 P_2} \;=\;& \frac{1}{4}(1+\cos^2\theta)\rho_{ijU}^{P_1 P_2} + \frac{1}{2}\sin^2\theta\,\rho_{ijL}^{P_1 P_2} + \frac{1}{2}\cos\theta\,\rho_{ijF}^{P_1 P_2} \\
& + \frac{1}{2}\sin\theta\cos\theta\,\rho_{ijI}^{P_1 P_2} + \frac{1}{2}\sin\theta\,\rho_{ijA}^{P_1 P_2},
\end{aligned} \quad (24)
$$

where the additional indices stand for unpolarised transverse (U), longitudinal (L), forward/backward asymmetric (F), longitudinal/transverse interference (I), and parity asymmetric (A) components of the intermediate (γ or Z) boson.

The top quarks decay almost immediately, and they can be detected via their decay products. The main decay channel is $t \rightarrow b + W^+$, where the W boson will decay into a quark–antiquark pair or into a pair consisting of charged lepton and neutrino. The latter is again the main channel, and the best particle to detect is the charged lepton. Thus the polarisation of the top quarks manifests itself through the angle between the momenta of charged lepton and antilepton, and also through respective angles between both of their momenta and the chosen basis. These angular dependencies, which are derived from hadronic collision [14], are written in article I as

$$\frac{1}{\sigma}\frac{d\sigma}{d\cos\theta_1 d\cos\theta_2} = \frac{1}{4}\left(1 + B_1\cos\theta_1 - B_2\cos\theta_2 - C\cos\theta_1\cos\theta_2\right), \quad (25)$$

where θ_1 and θ_2 are the angles between a fixed direction given by the basis used and the direction of flight of the charged lepton in the rest frames of the top and antitop quark, respectively, and

$$\frac{1}{\sigma}\frac{d\sigma}{d\phi} = \frac{1}{4}\left(1 - D\cos\phi\right),\tag{26}$$

where ϕ is the angle between the directions of flight $\hat{q}_1$ and $\hat{q}_2$ of the charged leptons in the rest frames of the top and antitop quark, respectively. The details of how experimentally measurable values can be attained from the aforementioned observables are shown in article I.

The opening angle ϕ between the two charged leptons is defined by $\hat{q}_1 \cdot \hat{q}_2 = \cos\phi$. In order to determine the distribution of the opening angle one has to integrate over all angles except for ϕ. One obtains

$$\frac{1}{8\pi^2}\int \mathrm{Tr}\left(\hat{\rho}(t\bar{t})\left(\hat{\rho}(t)\otimes\hat{\rho}(\bar{t})\right)\right)d\chi d\chi_1 d(\cos\theta_1)$$

$$= \rho(t)^2\rho\left(1 - \frac{1}{3}\left(\langle\mathcal{O}^{tt}\rangle + \langle\mathcal{O}^{nn}\rangle + \langle\mathcal{O}^{ll}\rangle\right)\cos\phi\right).\tag{27}$$

Therefore, the trace $\mathrm{Tr}\,\mathcal{O} = \mathcal{O}^{tt} + \mathcal{O}^{nn} + \mathcal{O}^{ll}$ of the three-dimensional correlation matrix in phase-space integrated form can be determined by measuring the distribution of the opening angle. The polar angle dependence of the trace is shown in Figure 3. Note that because this observable is equally derived from the trace of $\hat{\rho}$ with the tensor product of the spin operator with itself, the value is equal to 1 at LO (and at threshold) and decreases slightly (especially in backward direction) if we include NLO radiative corrections. Therefore, the dependence on $\cos\phi$ is at most $1/3$ of the integrated contribution.
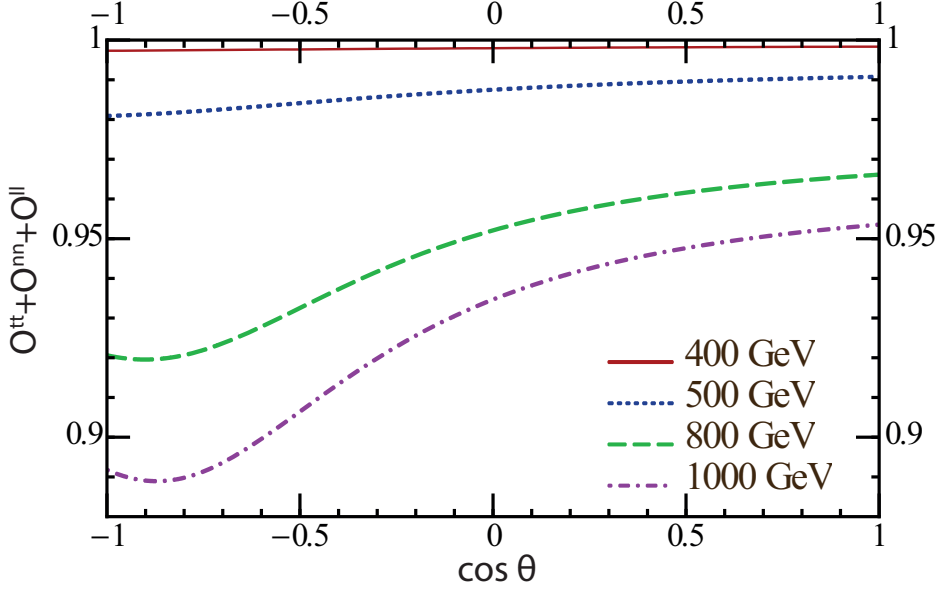
Figure 3: Trace $\mathrm{Tr}\,\mathcal{O}$ as a function of $\cos\theta$ for different energies $\sqrt{q^2} = 400\,\mathrm{GeV}$ (solid line), $500\,\mathrm{GeV}$ (dotted), $800\,\mathrm{GeV}$ (dashed), and $1000\,\mathrm{GeV}$ (dashed dotted)

3 Preface to Källén function and dilogarithms

3.1 Overview

Article II summarises some aspects related to the kinematics, and thus connects the respective parts of articles I and III. The main topic of article II is the appearance of the Källén function

$$\lambda(a, b, c) = a^2 + b^2 + c^2 - 2ab - 2ac - 2bc \tag{28}$$

in processes related to the interaction of three particles. The Källén function defines the kinematics, and it's arguments are the squares of (invariant) masses of the three particles. For example, the sign of the Källén function determines whether the process is real or virtual and thus generally also determines the integration domain. Article II examines more of these kinds of properties in depth.

3.2 Methodology

3.2.1 The appearance of the Källén function in kinematics

Let's examine a process where one particle with mass m_1 (e.g. a top quark) decays into two particles with masses m_2 and m_3 (e.g. W boson and bottom quark). We

18

make a simplifying assumption that all particles are real. If this assumption does not apply, the invariant masses need to be used instead. Even though the result is Lorentz invariant, we use the rest frame of the decaying particle, in which the momentum four-vector in the form of $p_1 = (m_1; 0, 0, 0)$. From the conservation of four-momentum we get $E_2 + E_3 = m_1$ and $\vec{p}_2 + \vec{p}_3 = \vec{0}$. In addition, for every particle there is the mass shell condition $m_2^2 = E_2^2 - \vec{p}_2^2$ and $m_3^2 = E_3^2 - \vec{p}_3^2$. Using $E_3 = m_1 - E_2$ and $\vec{p}_3^2 = \vec{p}_2^2$, all the parameters of the 3rd particle except for m_3 can be expressed by the parameters of the 2nd particle. The resulting system of equations can be solved for E_2 and E_3 to obtain

$$E_2 = \frac{m_1^2 + m_2^2 - m_3^2}{2m_1} \qquad \text{and}$$

$$E_3 = m_t - E_2 = \frac{m_1^2 - m_2^2 + m_3^2}{2m_1}. \tag{29}$$

For the (equal) squares of three-momenta we have

$$\vec{p}_2^2 = E_2^2 - m_2^2 = \lambda(m_1^2, m_2^2, m_3^2)/(4m_1^2) = E_3^2 - m_3^2 = \vec{p}_3^2. \tag{30}$$

While the denominators are determined by one particle being in the rest frame (i.e. the particle 1), the Källén function appears in the numerator of the squared three-momentum in every kinetic frame.

3.2.2 Dilogarithms

The dilogarithms appear naturally while integrating over the phase space, as is necessary and done in article I. In the result given for the coefficients $\rho^{e_1^i \bar{e}_2^j}$ in article I, one finds dilogarithms

$$\mathrm{Li}_2(z) = -\int_0^z \frac{\ln(1-u)}{u}\, \mathrm{d}u, \ z \in \mathbb{C} \setminus [1, \infty) \tag{31}$$

which are transcendental. The dilogarithms demand a particular care and tinkering due to their non-unique representation. There are relations between dilogarithms leading to transformations that convert a dilogarithm with one argument to a dilogarithm with another argument. The most important of these relations are

$$\mathrm{Li}_2(z) + \mathrm{Li}_2\left(\frac{1}{z}\right) = -\frac{\pi^2}{6} - \frac{1}{2}\ln^2(-z), \quad z \notin [0, 1[$$

$$\mathrm{Li}_2(z) + \mathrm{Li}_2(1 - z) = \frac{\pi^2}{6} - \ln z \ln(1 - z). \tag{32}$$

It is interesting to note that since both resulting transformations are involutions, there exist a hexagon orbit (33) which describes how to arrive from one dilogarithm argument to another.

$$
\begin{array}{ccc}
 & z & \\
\nearrow\swarrow & & \nwarrow\searrow \\
1-z & & \dfrac{1}{z} \\
\uparrow\downarrow & & \uparrow\downarrow \\
\dfrac{1}{1-z} & & 1-\dfrac{1}{z} \\
\nwarrow\searrow & & \nearrow\swarrow \\
 & \dfrac{-z}{1-z} &
\end{array}
\tag{33}
$$

Expressions involving dilogarithms may need to undergo several transformations to become manifestly real-valued. The same transformations can be used to group dilogarithms and to cancel similar terms. Such expressions have no definite shortest or simplest representation and expressions which are essentially identical may look very different.

3.3 Results

In article II it is shown how the appearance of the Källén function is the consequence of three particle kinematics and how the integration domain can be derived from the Källén function. Additionally, some useful substitutions are shown which are used in the calculations in articles I and III.

The relation to dilogarithms is found in that the arguments of the dilogarithms include the kinematics of the process and thus the Källén function. Besides the standard dilogarithm, there are also modifications of it. For example, the Bloch–Wigner dilogarithm is closely related to the Källén function and this connection is discussed in the second chapter of article II. The main result of the article are similarities between the Källén function and Bloch–Wigner dilogarithms which can be used as a simplifying approximation.

One of the results of article II is an approximation for the (transcendental) Bloch–Wigner dilogarithm given by the Källén function in equation (40) in article II. Unfortunately, a typographical error has occurred and this equation does not include the correct normalisation for the masses in the original version of article II. The correct equation reads

$$D\left(z(m_1^2, m_2^2, m_3^2)\right) \approx \frac{\sqrt{27}\,\text{Im}\left(\sqrt{\lambda(m_1^2, m_2^2, m_3^2)}\right)}{(m_1 + m_2 + m_3)^2}, \tag{34}$$

where the Bloch–Wigner dilogarithm is

$$D(z) = \text{Im}\left(\text{Li}_2(z) + \ln|z|\ln(1-z)\right) \tag{35}$$

and

$$z(m_1^2, m_2^2, m_3^2) = \frac{m_1^2 - m_2^2 + m_3^2 + \sqrt{\lambda(m_1^2, m_2^2, m_3^2)}}{2m_1^2}. \tag{36}$$

4 Preface to lepton mass effects in Higgs decay

4.1 Overview

One of the main aims for creating the LHC was to find and study the Higgs boson. Even though the proclamation of the discovery of the Higgs boson in 2012 [16, 17] may have seemed final to an outside observer, in reality the examination of the properties of the Higgs boson had just started. The mass, production and decay rates have been found consistent with Standard Model predictions [18]. Additional knowledge about the particle believed to be the Higgs boson can be attained by examining its decay processes.

Article III describes the τ-lepton mass effects to the overall rate and angular decay distribution of Higgs cascade decays $H \rightarrow Z(\rightarrow \ell^+\ell^-) + Z^*(\rightarrow \tau^+\tau^-)$ and $H \rightarrow W^-(\rightarrow \ell^-\bar{\nu}_\ell) + W^{+*}(\rightarrow \tau^+\nu_\tau)$ (see Figure 4) where one in the pair of gauge bosons is on mass shell (and, therefore, can be seen and identified as track in the detector) and its counterpart is not. The aim of these calculations is to examine the dependence of the results on the masses of final particles and the polarisations of intermediate particles using the helicity formalism. Theoretical results can be precisely compared to the experiment in order to examine the precision of the Standard Model including effects of mass and polarisation.
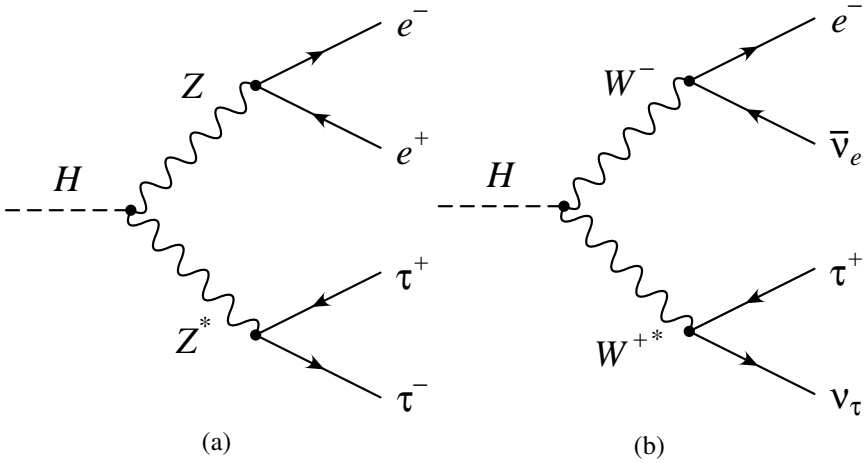

Figure 4: The Feynman diagrams of processes (a) $H \rightarrow Z(\rightarrow e^+e^-) + Z^*(\rightarrow \tau^+\tau^-)$ and (b) $H \rightarrow W^-(\rightarrow e^-\bar{\nu}_e) + W^{+*}(\rightarrow \tau^+\nu_\tau)$

4.2 Methodology

4.2.1 Energy and angular dependencies

The energies of the decay particles and the angular dependencies are examined in the decay process. For this purpose, five quantities are presented in article III, namely the invariant mass of the on-shell gauge boson $\sqrt{p^2}$, the polar angle θ_p between the direction of momentum of the gauge boson and the (positively) charged light fermion, the off-shell gauge boson invariant mass $\sqrt{q^2}$, the polar angle θ_q between the direction of momentum of gauge boson and (positively) charged heavy fermion, and the azimuthal angle between the two decay planes. The more complicated situation where the two gauge bosons are not distinguishable by their decay products either does not appear in case of the process $H \to WW$ at all because of the charges or, in the case of the process $H \to ZZ$, is removed from the discussion and will be examined in a future publication. Like the bracket notation implies, the conventions for processes $H \to ZZ$ and $H \to WW$ are slightly different (look at the figures in article III). The off-shell boson is the one which can decay through the tau channel (in case of Z^* it is $Z^* \to \tau^+\tau^-$ and in case of W^{+*} it is $W^{+*} \to \tau^+\nu_\tau$). In the discussion different energy and single angle dependencies are shown, and in comparison with the massless results the mass effect is revealed.

The angular dependencies can be disassembled by Legendre polynomials and in addition to differential decay rates, observables like convexity parameter and forward–backward asymmetry (for $H \to WW$) are defined and given in article III. The results are separated into helicity flip and helicity non-flip contributions based on whether the helicity (the projection of polarisation on the momentum vector) is conserved in the transition from vector boson to leptons or not.

4.2.2 Helicity formalism

There are two ways to reach the result: the direct route or the route via the helicity formalism. The helicity formalism enables the gauge boson contributions to be separated into vector and scalar parts, and the mass effects originate from the latter (which does not contribute in the on-shell case). The unitary gauge is used to prevent the appearance of Goldstone bosons. The boson propagator is split into

$$P_{0\oplus1}^{\nu\beta}(q) = -g^{\nu\beta} + \frac{q^\nu q^\beta}{m_V^2} = \underbrace{\left(-g^{\nu\beta} + \frac{q^\nu q^\beta}{q^2}\right)}_{\text{spin 1}} - \underbrace{\frac{q^\nu q^\beta}{q^2}F_S(q^2)}_{\text{spin 0}}, \quad (37)$$

where m_V is the mass of boson and

$$F_S(q^2) = \left(1 - \frac{q^2}{m_V^2}\right). \quad (38)$$

23

The propagators can be given in the helicity formalism as external products of the polarisation vector,

$$P_1^{\alpha\mu}(p) = \sum_{\lambda_V = \pm 1, 0} \bar{\varepsilon}^\alpha(\lambda_V)\bar{\varepsilon}^{*\,\mu}(\lambda_V) = -g^{\alpha\mu} + \frac{p^\alpha p^\mu}{p^2} \tag{39}$$

$(p^2 = m_V^2)$ and

$$P_{0\oplus 1}^{\mu'\alpha'}(q) = -\sum_{\lambda_{V^*} = t, \pm 1, 0} \varepsilon^{\mu'}(\lambda_{V^*})\varepsilon^{*\,\alpha'}(\lambda_{V^*})\,\hat{g}_{\lambda_{V^*}\lambda_{V^*}} = -g^{\mu'\alpha'} + \frac{q^{\mu'} q^{\alpha'}}{m_V^2}. \tag{40}$$

The polarisation vectors determine the helicity amplitudes,

$$H_{mn} = \bar{\varepsilon}^{*\,\alpha}(\lambda_V, p)H_{\alpha\alpha'}\varepsilon^{*\,\alpha'}(\lambda_{V^*}, q), \tag{41}$$

which are connected to the lepton and hadron tensors from article I in the form of

on-shell side: $\quad \bar{\varepsilon}^\alpha(\pm, p) = \dfrac{1}{\sqrt{2}}(0; \pm 1, -i, 0)$

$$\bar{\varepsilon}^\mu(0) = \frac{1}{\sqrt{p^2}\sqrt{(pq)^2 - p^2 q^2}}\left((pq)p^\mu - p^2 q^\mu\right) \qquad \bar{\varepsilon}^\mu(t) = \frac{p^\mu}{\sqrt{p^2}}$$

off-shell side: $\quad \varepsilon^\mu(\pm, q) = \dfrac{1}{\sqrt{2}}(0; \mp 1, -i, 0)$

$$\varepsilon^\mu(0) = \frac{1}{\sqrt{q^2}\sqrt{(pq)^2 - p^2 q^2}}\left((pq)q^\mu - q^2 p^\mu\right) \qquad \varepsilon^\mu(t) = \frac{q^\mu}{\sqrt{q^2}} \tag{42}$$

Using $H_{\alpha\alpha'} = g_{\alpha\alpha'}$ in case of the Standard Model we arrive at

$$H_{++} = H_{--} = 1, \qquad H_{00} = H_{tt} = \frac{pq}{\sqrt{p^2}\sqrt{q^2}},$$

$$H_{0t} = H_{t0} = \frac{\sqrt{(pq)^2 - p^2 q^2}}{\sqrt{p^2}\sqrt{q^2}} = \frac{m_H |\vec{p}_V|}{\sqrt{p^2}\sqrt{q^2}}. \tag{43}$$

The results are given by bilinear forms consisting of helicity amplitudes

$$\begin{aligned}
\rho_{00} &= |H_{00}|^2, & \rho_{\pm\pm} &= |H_{\pm\pm}|^2, & \rho_{tt} &= \operatorname{Re} H_{0t}H_{0t}^*, \\
\rho_{\pm 0} &= \operatorname{Re} H_{\pm\pm}H_{00}^*, & \rho_{\pm\mp} &= \operatorname{Re} H_{\pm\pm}H_{\mp\mp}^*, \\
\rho_{\pm t} &= \operatorname{Re} H_{\pm\pm}H_{0t}^*, & \rho_{t\pm} &= \operatorname{Re} H_{0t}H_{\pm\pm}^*, \\
\rho_{0t} &= \operatorname{Re} H_{00}H_{0t}^*, & \rho_{t0} &= \operatorname{Re} H_{t0}H_{00}^*.
\end{aligned} \tag{44}$$

Compared to these the helicity amplitudes related to the lepton tensor are in a simpler form. The angular dependence comes from the Wigner d-function, and the connection to the system given in article I is given by

$$\rho_U = \rho_{++} + \rho_{--}, \quad \rho_L = \rho_{00} \quad \text{and} \quad \rho_S = \rho_{tt}. \tag{45}$$

All contributions except for the last (scalar) one are already known from article I (cf. Section 2). The resolution into U, L, and S parts is evident for every observable, both in case of massless and massive leptons.

4.2.3 Analytical vs. numerical calculations

Differential decay rates that depend on the invariant masses of the gauge bosons can be calculated analytically, whereas in the calculation of the process with three masses (m_H, $\sqrt{p^2}$ and $\sqrt{q^2}$) once again the Källén function appears. Only when it becomes necessary to integrate over the invariant mass of the second boson (which is off-shell), we need numeric integration. For this purpose we use a well-known Monte Carlo program called VEGAS [19] which is fast and reliable, and also double-check with Mathematica's numeric integration.

4.3 Results

Lepton mass effects are evident in the off-shell decays $Z^* \to \tau^+ \tau^-$ and $W^{+*} \to \tau^+ \nu_\tau$. Lepton mass effects are larger for the $H \to ZZ^*$ mode where a reduction of $3.97\,\%$ in the decay rate to τ relative to the decay rates to e or μ is found (see figures 5 and 6).

The important point is that in case of off-shell decay the scalar and longitudinal-scalar interference contributions are no longer on scale with the square of lepton mass which could be neglected at the scale of $m_{W,Z}^2$. Instead they depend on the off-shellness of respective gauge bosons which is limited by the zero recoil point $q^2 = (m_H - m_{W,Z})^2$. In low energy calculations one usually drops the term $q^2/m_{W,Z}^2$, since $q^2 \ll m_{W,Z}^2$, but in case of the decay process considered in article III the factor $q^2/m_{W,Z}^2$ can be as large as 30% at the zero recoil point.

The rate reduction due to lepton mass effects is significantly larger at the lower end of the q^2 spectrum where the ratio of m_τ^2 to q^2 is larger. In the charged-current case one finds a non-vanishing forward–backward asymmetry in the $\cos\theta_q$ distribution through lepton mass induced scalar–longitudinal interference effects. The forward–backward asymmetry can become quite large in the low-q^2 region.
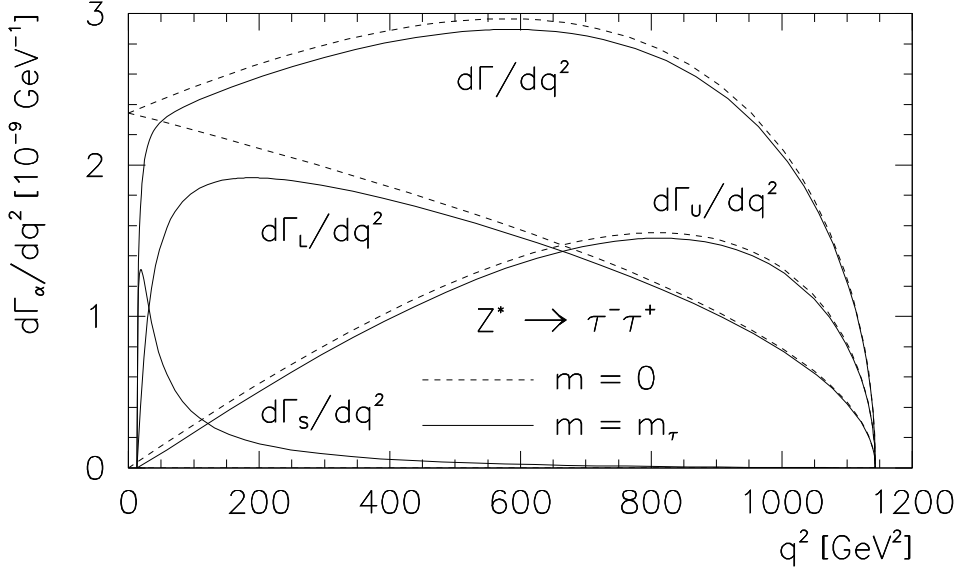
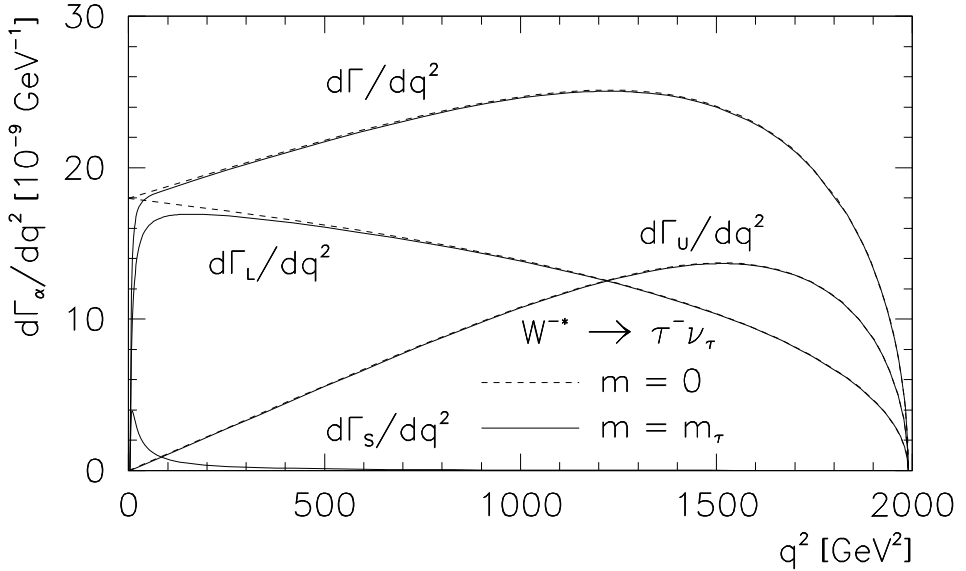Figure 5: Differential rates $d\Gamma_\alpha^Z/dq^2$ for the decay $H \to Z(\to e^+e^-) + Z^*(\to \ell^+\ell^-)$ with $m_\ell = 0$ and $m_\ell = m_\tau$

Figure 6: Differential rates $d\Gamma_\alpha^W/dq^2$ for the decay $H \to W^-(\to e^-\bar{\nu}_e) + W^{+*}(\to \ell^+\nu_\ell)$ with $m_\ell = 0$ and $m_\ell = m_\tau$

26

5 Summary

Particle physics research related to the LHC and CLIC/ILC colliders is one of the major areas of modern science. The theoretical calculations presented in this thesis are connected to elementary particle collisions in these colliders.

The thesis consists of two main topics. The first topic focuses on the spin–spin correlation of a top and antitop quark pair created in an electron–positron annihilation. Article I provides analytical Standard Model results describing the first order $O(\alpha_s)$ corrections to the double spin density matrix elements of such a quark pair in the beam frame spanned by the momenta of the electron and the quark. The correlation of combinations of longitudinal, transverse and normal spin orientations are studied. A possible method for measuring spin–spin correlations through an angular analysis of the polarized quark decays based on spin–spin density formalism is discussed. Furthermore, a way to generalise the results to the case of polarized electron–positron annihilation is provided.

The other topic is lepton mass effects in Higgs boson decay presented in article III. Considered are the four-body decays $H \rightarrow Z(\rightarrow \ell^+\ell^-) + Z^*(\rightarrow \tau^+\tau^-)$ and $H \rightarrow W^-(\rightarrow \ell^-\bar{\nu}_\ell) + W^{+*}(\rightarrow \tau^+\nu_\tau)$, where one in the pair of the gauge bosons is on mass shell and its counterpart is not. The inclusion of τ lepton mass effects explains an overall rate reduction relative to the zero mass case. The reduction is larger for the ZZ^* case. From the energy-dependence perspective the rate reduction is significantly larger at the lower end of energy spectrum near the zero recoil point. In the charged-current case one finds a non-vanishing forward–backward asymmetry in the angular distribution through lepton mass induced scalar–longitudinal interference effects.

The results of both studies are given analytically as angular decay distributions and partial rates in the helicity formalism. This allows to analyse dependencies on different parameters in detail and to calculate the behaviour in different kinematical limits. Taking into account mass and spin polarisation effects for the decay products, our results help to guide future experiments and enable a more detailed comparison with the Standard Model. Both topics also encompass massive particles decays that employ the Källén function which is examined in relation to dilogarithms in article II.

Kokkuvõte (Summary in Estonian)

Fermionite spinni polarisatsiooni ja massi mõju top-kvargipaari tekkel ja Higgsi bosoni lagunemisel

Tänapäeva teaduse üks suuremaid valdkondi on osakestefüüsika, mis hõlmab endas ka LHC-ga (suur hadronite põrguti) ja CLIC-ga (kompaktne lineaarne põrguti) ning ILC-ga (rahvusvaheline lineaarne põrguti) seonduvat. Käesolevas väitekirjas kirjeldatud teoreetilised arvutused on seotud elementaarosakeste põrgetega neis kiirendites.

Käesolev väitekiri sisaldab kahte põhilist teemat. Esimene teema keskendub elektroni ja positroni annihileerumisel tekkinud top-antitop-kvargipaari spinn-spinn-korrelatsioonile. Artikkel I annab Standardmudeli järgi arvutatud analüütilised tulemused, mis kirjeldavad esimest järku $O(\alpha_s)$-parandeid sellise kvargipaari spinn-spinn-kaksiktihedusmaatriksi elementidele elektronkiire ja kvargi poolt määratud taustsüsteemis. Uuritakse spinni piki- ja ristisuunaliste orientatsioonide kombinatsioonide korrelatsioone. Käsitletakse spinn-spinn-korrelatsioonide mõõtmise võimalust polariseeritud kvargi lagunemisproduktide liikumissuundade nurkade abil kasutades tihedusformalismi. Lisaks sellele antakse viis, kuidas üldistada antud tulemusi polariseeritud elektron- ja positronkiirte korral.

Teine teema on leptonmassi efektid Higgsi bosoni lagunemisel artiklis III. Nimelt saab Higgsi boson laguneda neljaks osakeseks läbi Z-bosoni paari $H \rightarrow Z(\rightarrow \ell^+\ell^-) + Z^*(\rightarrow \tau^+\tau^-)$ ja W-bosoni paari $H \rightarrow W^-(\rightarrow \ell^-\bar{\nu}_\ell) + W^{+*}(\rightarrow \tau^+\nu_\tau)$, kusjuures üks vahebosonitest on massipinnal ja selle teisik ei ole. τ-leptoni massi arvessevõtmine annab kogu reaktsiooni ristlõike vähenemise võrreldes leptoni massi mittearvestamisega. Vähenemine on suurem ZZ^* korral. Energiasõltuvuse vaatenurgast on ristlõike vähenemine märkimisväärselt suurem energiaspektri madalamas otsas, kus massipinnal olev boson on paigal. W-bosoni korral ilmneb nurkjaotuses mittekaduv edasi-tagasisuunaline asümmeetria, mis on tingitud leptoni massi poolt tekitatud skalaarse ja pikipanuse interferentsist.

Mõlema teema uurimistulemused on antud analüütiliselt lagunemise nurkjaotustena ja osaliste ristlõigetena helitsiteetsusformalismis. See võimaldab täpsemalt uurida sõltuvust erinevatest parameetritest ja arvutada tulemuste käitumist erinevatel piirjuhtudel. Need leiud heidavad valgust massi- ja spinniefektidele osakeste lagunemisel ja sellest juhinduvalt saab tulevastes eksperimentides läbi viia täpsemaid võrdlusi Standardmudeliga. Mõlemad teemad hõlmavad massiga osakeste lagunemist, mille arvutamise käigus rakendatakse Källén funktsiooni, mida ja mille seost dilogaritmidega uuritakse lähemalt artiklis II.

References

[1] M.E. Peskin and D.V. Schroeder,
An Introduction to Quantum Field Theory (Westview Press 1995)

[2] B. Odom, D. Hanneke, B. D'Urso, and G. Gabrielse,
"New Measurement of the Electron Magnetic Moment Using a One-Electron Quantum Cyclotron," *Phys. Rev. Lett.* **97** (2006) 030801

[3] K. Fujii *et al.* [LCC Physics Working Group], "Physics Case for the International Linear Collider," arXiv:1506.05992v2 [hep-ph]

[4] M.J. Boland *et al.* [The CLIC and CLICdp collaborations], "Updated baseline for a staged Compact Linear Collider," arXiv:1608.07537v2 [hep-ph]

[5] A.G. Drutskoy, "Physics at ILC," *J. Phys.: Conf. Ser.* **675** (2016) 022019

[6] M. Böhm, A. Denner and H. Joos, *Gauge Theories of the Strong and Electroweak Interaction* (B.G. Teubner Stuttgart 2001)

[7] K. Aoki, Z. Hioki, R. Kawabe, M. Konuma, and T. Muta, "Electroweak Theory – Framework of On-Shell Renormalization and Study of Higher-Order Effects," *Progress of Theoretical Physics Supp* **73** (1982) p. 1-226

[8] S. Groote, J.G. Körner and M.M. Tung, "Polar angle dependence of the alignment polarization of quarks produced in e^+e^- annihilation,"
Z. Phys. **C74** (1997) 615

[9] J.G. Körner and D.H. Schiller, "Helicity description of $e^+ e^- \to q$ anti-q g and $e^+ e^- \to q$ anti-$q \to g$ g g on and off the Z_0: quark, gluon and beam polarization effects," DESY-81-043.

[10] E. Leader, *Spin in particle physics* (Cambridge University Press 2001)

[11] A. Brandenburg, M. Flesch and P. Uwer, "The Spin density matrix of top quark pairs produced in electron–positron annihilation including QCD radiative corrections," *Phys. Rev.* **D59** (1999) 014001

[12] A. Brandenburg, M. Flesch and P. Uwer, "Polarization and spin correlations of top quarks at a future $e^+ e^-$ linear collider,"
Czech. J. Phys. **50S1** (2000) 51

[13] S. Groote, J.G. Körner, B. Melić and S. Prelovsek, "A survey of top quark polarization at a polarized linear $e^+ e^-$ collider,"
Phys. Rev. **D83** (2011) 054018

[14] W. Bernreuther, A. Brandenburg, Z.G. Si and P. Uwer, "Top quark pair production and decay at hadron colliders," *Nucl. Phys.* **B690** (2004) 81

[15] S. Groote, W.S. Huo, A. Kadeer and J.G. Körner, "Azimuthal correlation between the $(\vec{p}_\ell, \vec{p}_{X_b})$ and $(\vec{p}_\ell, \vec{P}_t)$ planes in the semileptonic rest frame decay of a polarized top quark: An $O(\alpha_s)$ effect," *Phys. Rev.* **D76** (2007) 014012

[16] G. Aad *et al.* [ATLAS Collaboration], "Observation of a new particle in the search for the Standard Model Higgs boson with the ATLAS detector at the LHC," *Phys. Lett.* **B716** (2012) 1

[17] S. Chatrchyan *et al.* [CMS Collaboration], "Observation of a new boson at a mass of 125 GeV with the CMS experiment at the LHC," *Phys. Lett.* **B716** (2012) 30

[18] C. Patrignani *et al.* [Particle Data Group Collaboration], "Review of Particle Physics," *Chin. Phys.* C **40** (2016) 100001

[19] G.P. Lepage, "A New Algorithm for Adaptive Multidimensional Integration," *Journal of Computational Physics* **27** (1978) p. 192-203

Publications

Curriculum vitae

General

Given name	**Lauri**
Family name	**Kaldamäe**
Date of birth	13.05.1987
Address	Pikk 19-56, Tartu
Phone number	55600254
E-mail	kaldamae@ut.ee

Education

2011 – 2017	University of Tartu, Doctor of Philosophy (Physics)
2009 – 2011	University of Tartu, Master of Science (Nanotechnology / Solid state physics)
2006 – 2009	University of Tartu, Bachelor of Science (Fundamental physics)
2003 – 2006	Tallinn Secondary Science School

Work experience

since 2017	CGI Estonia – software developer
2006 – 2017	Technical Translation Centre – software developer
2011 – 2016	Estonian Physical Society – editor/translator
2011 – 2013	Estonian Physical Society – teacher
2009 – 2011	Estonian Nanotechnology Competence Centre – lab worker
2006 – 2011	Member of science bus "Suur Vanker"

Publications

I L. Kaldamäe, S. Groote, J. G. Körner, Analytical $O(\alpha_s)$ corrections to the beam frame double-spin density matrix elements of $e^+e^- \to t\bar{t}$, Physical Review **D94** (2016) 114003

II L. Kaldamäe, S. Groote, Virtual and real processes, the Källén function, and the relation to dilogarithms, Journal of Physics G: Nuclear and Particle Physics **42** (2015) 085003

III S. Berge, S. Groote, J. G. Körner, L. Kaldamäe, Lepton-mass effects in the decays $H \to ZZ^* \to \ell^+\ell^-\tau^+\tau^-$ and $H \to WW^* \to \ell\nu\tau\nu_\tau$, Physical Review **D92** (2015) 033001

Elulookirjeldus (Curriculum vitae in Estonian)

Üldandmed

Eesnimi	**Lauri**
Perekonnanimi	**Kaldamäe**
Sünniaeg	13.05.1987
Aadress	Pikk 19-56, Tartu
Telefon	55600254
E-post	kaldamae@ut.ee

Haridustee

2011 – 2017	Tartu Ülikool, filosoofiadoktor (füüsika)
2009 – 2011	Tartu Ülikool, loodusteaduste magister (nanotehnoloogia/tahkisefüüsika)
2006 – 2009	Tartu Ülikool, loodusteaduste bakalaureus (fundamentaalfüüsika)
2003 – 2006	Tallinna Reaalkool

Töökogemus

alates 2017	CGI Eesti – programmeerija
2006 – 2017	Tehnilise Tõlke Keskus – programmeerija
2011 – 2016	Eesti Füüsika Selts – toimetaja/tõlkija
2011 – 2013	Eesti Füüsika Selts – õpetaja
2009 – 2011	Eesti Nanotehnoloogiate Arenduskeskuse AS – laborant
2006 – 2011	Teadusbussi "Suur Vanker" liige

Publikatsioonid

I L. Kaldamäe, S. Groote, J. G. Körner, Analytical $O(\alpha_s)$ corrections to the beam frame double-spin density matrix elements of $e^+e^- \to t\bar{t}$, Physical Review **D94** (2016) 114003

II L. Kaldamäe, S. Groote, Virtual and real processes, the Källén function, and the relation to dilogarithms, Journal of Physics G: Nuclear and Particle Physics **42** (2015) 085003

III S. Berge, S. Groote, J. G. Körner, L. Kaldamäe, Lepton-mass effects in the decays $H \to ZZ^* \to \ell^+\ell^-\tau^+\tau^-$ and $H \to WW^* \to \ell\nu\tau\nu_\tau$, Physical Review **D92** (2015) 033001

DISSERTATIONES PHYSICAE
UNIVERSITATIS TARTUENSIS

1. **Andrus Ausmees.** XUV-induced electron emission and electron-phonon interaction in alkali halides. Tartu, 1991.
2. **Heiki Sõnajalg.** Shaping and recalling of light pulses by optical elements based on spectral hole burning. Tartu, 1991.
3. **Sergei Savihhin.** Ultrafast dynamics of F-centers and bound excitons from picosecond spectroscopy data. Tartu, 1991.
4. **Ergo Nõmmiste.** Leelishalogeniidide röntgenelektronemissioon kiiritamisel footonitega energiaga 70–140 eV. Tartu, 1991.
5. **Margus Rätsep.** Spectral gratings and their relaxation in some low-temperature impurity-doped glasses and crystals. Tartu, 1991.
6. **Tõnu Pullerits.** Primary energy transfer in photosynthesis. Model calculations. Tartu, 1991.
7. **Olev Saks.** Attoampri diapasoonis voolude mõõtmise füüsikalised alused. Tartu, 1991.
8. **Andres Virro.** AlGaAsSb/GaSb heterostructure injection lasers. Tartu, 1991.
9. **Hans Korge.** Investigation of negative point discharge in pure nitrogen at atmospheric pressure. Tartu, 1992.
10. **Jüri Maksimov.** Nonlinear generation of laser VUV radiation for high-resolution spectroscopy. Tartu, 1992.
11. **Mark Aizengendler.** Photostimulated transformation of aggregate defects and spectral hole burning in a neutron-irradiated sapphire. Tartu, 1992.
12. **Hele Siimon.** Atomic layer molecular beam epitaxy of A^2B^6 compounds described on the basis of kinetic equations model. Tartu, 1992.
13. **Tõnu Reinot.** The kinetics of polariton luminescence, energy transfer and relaxation in anthracene. Tartu, 1992.
14. **Toomas Rõõm.** Paramagnetic H^{2-} and F^+ centers in CaO crystals: spectra, relaxation and recombination luminescence. Tallinn, 1993.
15. **Erko Jalviste.** Laser spectroscopy of some jet-cooled organic molecules. Tartu, 1993.
16. **Alvo Aabloo.** Studies of crystalline celluloses using potential energy calculations. Tartu, 1994.
17. **Peeter Paris.** Initiation of corona pulses. Tartu, 1994.
18. **Павел Рубин.** Локальные дефектные состояния в CuO_2 плоскостях высокотемпературных сверхпроводников. Тарту, 1994.
19. **Olavi Ollikainen.** Applications of persistent spectral hole burning in ultrafast optical neural networks, time-resolved spectroscopy and holographic interferometry. Tartu, 1996.
20. **Ülo Mets.** Methodological aspects of fluorescence correlation spectroscopy. Tartu, 1996.
21. **Mikhail Danilkin.** Interaction of intrinsic and impurity defects in CaS:Eu luminophors. Tartu, 1997.

22. **Ирина Кудрявцева.** Создание и стабилизация дефектов в кристаллах KBr, KCl, RbCl при облучении ВУФ-радиацией. Тарту, 1997.
23. **Andres Osvet.** Photochromic properties of radiation-induced defects in diamond. Tartu, 1998.
24. **Jüri Örd.** Classical and quantum aspects of geodesic multiplication. Tartu, 1998.
25. **Priit Sarv.** High resolution solid-state NMR studies of zeolites. Tartu, 1998.
26. **Сергей Долгов.** Электронные возбуждения и дефектообразование в некоторых оксидах металлов. Тарту, 1998.
27. **Kaupo Kukli.** Atomic layer deposition of artificially structured dielectric materials. Tartu, 1999.
28. **Ivo Heinmaa.** Nuclear resonance studies of local structure in $RBa_2Cu_3O_{6+x}$ compounds. Tartu, 1999.
29. **Aleksander Shelkan.** Hole states in CuO_2 planes of high temperature superconducting materials. Tartu, 1999.
30. **Dmitri Nevedrov.** Nonlinear effects in quantum lattices. Tartu, 1999.
31. **Rein Ruus.** Collapse of 3d (4f) orbitals in 2p (3d) excited configurations and its effect on the x-ray and electron spectra. Tartu, 1999.
32. **Valter Zazubovich.** Local relaxation in incommensurate and glassy solids studied by Spectral Hole Burning. Tartu, 1999.
33. **Indrek Reimand.** Picosecond dynamics of optical excitations in GaAs and other excitonic systems. Tartu, 2000.
34. **Vladimir Babin.** Spectroscopy of exciton states in some halide macro- and nanocrystals. Tartu, 2001.
35. **Toomas Plank.** Positive corona at combined DC and AC voltage. Tartu, 2001.
36. **Kristjan Leiger.** Pressure-induced effects in inhomogeneous spectra of doped solids. Tartu, 2002.
37. **Helle Kaasik.** Nonperturbative theory of multiphonon vibrational relaxation and nonradiative transitions. Tartu, 2002.
38. **Tõnu Laas.** Propagation of waves in curved spacetimes. Tartu, 2002.
39. **Rünno Lõhmus.** Application of novel hybrid methods in SPM studies of nanostructural materials. Tartu, 2002.
40. **Kaido Reivelt.** Optical implementation of propagation-invariant pulsed free-space wave fields. Tartu, 2003.
41. **Heiki Kasemägi.** The effect of nanoparticle additives on lithium-ion mobility in a polymer electrolyte. Tartu, 2003.
42. **Villu Repän.** Low current mode of negative corona. Tartu, 2004.
43. **Алексей Котлов.** Оксианионные диэлектрические кристаллы: зонная структура и электронные возбуждения. Tartu, 2004.
44. **Jaak Talts.** Continuous non-invasive blood pressure measurement: comparative and methodological studies of the differential servo-oscillometric method. Tartu, 2004.
45. **Margus Saal.** Studies of pre-big bang and braneworld cosmology. Tartu, 2004.

46. **Eduard Gerškevitš.** Dose to bone marrow and leukaemia risk in external beam radiotherapy of prostate cancer. Tartu, 2005.
47. **Sergey Shchemelyov.** Sum-frequency generation and multiphoton ionization in xenon under excitation by conical laser beams. Tartu, 2006.
48. **Valter Kiisk.** Optical investigation of metal-oxide thin films. Tartu, 2006.
49. **Jaan Aarik.** Atomic layer deposition of titanium, zirconium and hafnium dioxides: growth mechanisms and properties of thin films. Tartu, 2007.
50. **Astrid Rekker.** Colored-noise-controlled anomalous transport and phase transitions in complex systems. Tartu, 2007.
51. **Andres Punning.** Electromechanical characterization of ionic polymer-metal composite sensing actuators. Tartu, 2007.
52. **Indrek Jõgi.** Conduction mechanisms in thin atomic layer deposited films containing TiO_2. Tartu, 2007.
53. **Aleksei Krasnikov.** Luminescence and defects creation processes in lead tungstate crystals. Tartu, 2007.
54. **Küllike Rägo.** Superconducting properties of MgB_2 in a scenario with intra- and interband pairing channels. Tartu, 2008.
55. **Els Heinsalu.** Normal and anomalously slow diffusion under external fields. Tartu, 2008.
56. **Kuno Kooser.** Soft x-ray induced radiative and nonradiative core-hole decay processes in thin films and solids. Tartu, 2008.
57. **Vadim Boltrushko.** Theory of vibronic transitions with strong nonlinear vibronic interaction in solids. Tartu, 2008.
58. **Andi Hektor.** Neutrino Physics beyond the Standard Model. Tartu, 2008.
59. **Raavo Josepson.** Photoinduced field-assisted electron emission into gases. Tartu, 2008.
60. **Martti Pärs.** Study of spontaneous and photoinduced processes in molecular solids using high-resolution optical spectroscopy. Tartu, 2008.
61. **Kristjan Kannike.** Implications of neutrino masses. Tartu, 2008.
62. **Vigen Issahhanjan.** Hole and interstitial centres in radiation-resistant MgO single crystals. Tartu, 2008.
63. **Veera Krasnenko.** Computational modeling of fluorescent proteins. Tartu, 2008.
64. **Mait Müntel.** Detection of doubly charged higgs boson in the CMS detector. Tartu, 2008.
65. **Kalle Kepler.** Optimisation of patient doses and image quality in diagnostic radiology. Tartu, 2009.
66. **Jüri Raud.** Study of negative glow and positive column regions of capillary HF discharge. Tartu, 2009.
67. **Sven Lange.** Spectroscopic and phase-stabilisation properties of pure and rare-earth ions activated ZrO_2 and HfO_2. Tartu, 2010.
68. **Aarne Kasikov.** Optical characterization of inhomogeneous thin films. Tartu, 2010.
69. **Heli Valtna-Lukner.** Superluminally propagating localized optical pulses. Tartu, 2010.

70. **Artjom Vargunin.** Stochastic and deterministic features of ordering in the systems with a phase transition. Tartu, 2010.
71. **Hannes Liivat.** Probing new physics in e+e− annihilations into heavy particles via spin orientation effects. Tartu, 2010.
72. **Tanel Mullari.** On the second order relativistic deviation equation and its applications. Tartu, 2010.
73. **Aleksandr Lissovski.** Pulsed high-pressure discharge in argon: spectroscopic diagnostics, modeling and development. Tartu, 2010.
74. **Aile Tamm.** Atomic layer deposition of high-permittivity insulators from cyclopentadienyl-based precursors. Tartu, 2010.
75. **Janek Uin.** Electrical separation for generating standard aerosols in a wide particle size range. Tartu, 2011.
76. **Svetlana Ganina.** Hajusandmetega ülesanded kui üks võimalus füüsika-õppe efektiivsuse tõstmiseks. Tartu, 2011
77. **Joel Kuusk.** Measurement of top-of-canopy spectral reflectance of forests for developing vegetation radiative transfer models. Tartu, 2011.
78. **Raul Rammula**. Atomic layer deposition of HfO_2 – nucleation, growth and structure development of thin films. Tartu, 2011.
79. **Сергей Наконечный.** Исследование электронно-дырочных и интерстициал-вакансионных процессов в монокристаллах MgO и LiF методами термоактивационной спектроскопии. Тарту, 2011.
80. **Niina Voropajeva.** Elementary excitations near the boundary of a strongly correlated crystal. Tartu, 2011.
81. **Martin Timusk.** Development and characterization of hybrid electro-optical materials. Tartu, 2012, 106 p.
82. **Merle Lust.** Assessment of dose components to Estonian population. Tartu, 2012, 84 p.
83. **Karl Kruusamäe.** Deformation-dependent electrode impedance of ionic electromechanically active polymers. Tartu, 2012, 128 p.
84. **Liis Rebane.** Measurement of the $W \rightarrow \tau\nu$ cross section and a search for a doubly charged Higgs boson decaying to τ-leptons with the CMS detector. Tartu, 2012, 156 p.
85. **Jevgeni Šablonin.** Processes of structural defect creation in pure and doped MgO and NaCl single crystals under condition of low or super high density of electronic excitations. Tartu, 2013, 145 p.
86. **Riho Vendt**. Combined method for establishment and dissemination of the international temperature scale. Tartu, 2013, 108 p.
87. **Peeter Piksarv.** Spatiotemporal characterization of diffractive and non-diffractive light pulses. Tartu, 2013, 156 p.
88. **Anna Šugai.** Creation of structural defects under superhigh-dense irradiation of wide-gap metal oxides. Tartu, 2013, 108 p.
89. **Ivar Kuusik.** Soft X-ray spectroscopy of insulators. Tartu, 2013, 113 p.
90. **Viktor Vabson**. Measurement uncertainty in Estonian Standard Laboratory for Mass. Tartu, 2013, 134 p.

91. **Kaupo Voormansik.** X-band synthetic aperture radar applications for environmental monitoring. Tartu, 2014, 117 p.
92. **Deivid Pugal.** hp-FEM model of IPMC deformation. Tartu, 2014, 143 p.
93. **Siim Pikker.** Modification in the emission and spectral shape of photo-stable fluorophores by nanometallic structures. Tartu, 2014, 98 p.
94. **Mihkel Pajusalu**. Localized Photosynthetic Excitons. Tartu, 2014, 183 p.
95. **Taavi Vaikjärv.** Consideration of non-adiabaticity of the Pseudo-Jahn-Teller effect: contribution of phonons. Tartu, 2014, 129 p.
96. **Martin Vilbaste.** Uncertainty sources and analysis methods in realizing SI units of air humidity in Estonia. Tartu, 2014, 111 p.
97. **Mihkel Rähn.** Experimental nanophotonics: single-photon sources- and nanofiber-related studies. Tartu, 2015, 107 p.
98. **Raul Laasner.** Excited state dynamics under high excitation densities in tungstates. Tartu, 2015, 125 p.
99. **Andris Slavinskis.** EST Cube-1 attitude determination. Tartu, 2015, 104 p.
100. **Karlis Zalite**. Radar Remote Sensing for Monitoring Forest Floods and Agricultural Grasslands. Tartu, 2016, 124 p.
101. **Kaarel Piip.** Development of LIBS for *in-situ* study of ITER relevant materials. Tartu, 2016, 93 p.
102. **Kadri Isakar.** ^{210}Pb in Estonian air: long term study of activity concentrations and origin of radioactive lead. Tartu, 2016, 107 p.
103. **Artur Tamm.** High entropy alloys: study of structural properties and irradiation response. Tartu, 2016, 115 p.
104. **Rasmus Talviste.** Atmospheric-pressure He plasma jet: effect of dielectric tube diameter. Tartu, 2016, 107 p.
105. **Andres Tiko.** Measurement of single top quark properties with the CMS detector. Tartu, 2016, 161 p.
106. **Aire Olesk.** Hemiboreal Forest Mapping with Interferometric Synthetic Aperture Radar. Tartu, 2016, 121 p.
107. **Fred Valk.** Nitrogen emission spectrum as a measure of electric field strength in low-temperature gas discharges. Tartu, 2016, 149 p.
108. **Manoop Chenchiliyan.** Nano-structural Constraints for the Picosecond Excitation Energy Migration and Trapping in Photosynthetic Membranes of Bacteria. Tartu, 2016, 115p.